



EVALUATION OF LIQUEFACTION RESISTANCE OF COMPACTED GROUND BY FIELD VIBRATION TEST

K. Harada⁽¹⁾, T. Ito⁽²⁾, K. Yamashita⁽³⁾, R.P. Orense⁽⁴⁾

⁽¹⁾ Duty Manager, Fudo Tetra Corporation, Japan, kenji.harada@fudotetra.co.jp

⁽²⁾ Senior Engineer, Fudo Tetra Corporation, Japan, takeshi.ito@fudotetra.co.jp

⁽³⁾ Senior Engineer, Fudo Tetra Corporation, Japan, katsuji.yamashita@fudotetra.co.jp

⁽⁴⁾ Associate Professor, University of Auckland, NZ, r.orense@auckland.ac.nz

Abstract

The evaluation of the liquefaction resistance of compacted ground, such as by the sand compaction pile (SCP) method, is performed by considering the N-value from standard penetration test obtained between the sand piles which is the weakest point. Therefore, under this condition, the liquefaction resistance cannot be evaluated appropriately as the composite ground effect due to the existence of the compacted sand pile and the increase in lateral stress induced at the time of sand pile installation are not taken into account. In addition, the liquefaction resistance determined from the results of subjecting samples, obtained by push tube sampling between the sand piles, to laboratory tests such as cyclic undrained triaxial tests may underestimate the in-situ resistance of the compacted ground because of possible effect of disturbance (loosening) during sampling and transport. Since the current design procedure evaluates the liquefaction resistance of the improved ground with respect to the increase in the relative density, it can be surmised that the actual liquefaction resistance is not properly evaluated; however, if it can be estimated directly in-situ, such problem may be resolved.

In this paper, in order to estimate the in-situ liquefaction resistance of the compacted ground, the results of vibration tests conducted previously at four sites using the vibro hammer of SCP method are re-analyzed and the relationship between the maximum shear stress ratio, L_{\max} , and the maximum excess pore water pressure ratio, $r_{u,\max}$, is plotted. From the chart, it is observed that for the same corrected SPT N-value N_{cs} , the pore water pressure development is different between the natural ground and the compacted ground, with the latter being more effective in suppressing the generation of pore water pressure for the same level of ground shaking. This observation indicates that, for the same level of shear stress induced by earthquake shaking and for the same SPT N-value obtained by analysis or from numerical simulation, the compacted ground has larger liquefaction resistance when compared to the original ground.

Keywords: liquefaction resistance; compacted ground; vibration test; SCP method



1. Introduction

The evaluation of the liquefaction resistance of ground improved by sand compaction pile method (hereinafter referred to as the “improved ground”) is usually performed using the standard penetration test (SPT) N-value obtained between the piles. However, since the relationship between the liquefaction resistance of the ground and the penetration resistance (i.e. the N value) assumes that the static earth pressure coefficient, K_0 , of the ground is 0.5, the resistance is deemed to be underestimated because any increase in the K_0 value as a result of sand pile installation is not considered. In addition, the liquefaction resistance obtained from the laboratory test results, such as from undrained cyclic triaxial tests, on tube-sampled specimens of the improved ground indicates that the potential disturbance of the specimen during sampling and transport may result in underestimation of the in-situ liquefaction resistance [1]. Furthermore, the actual improved ground is a composite ground consisting of multiple compacted sand piles and the ground in-between the piles, and the liquefaction resistance between the piles does not reflect the composite ground effect due to the presence of sand piles. Hence, as described above, the current design procedure evaluates only the effect of density increase on the liquefaction resistance of the improved ground and therefore it can be surmised that such resistance has not been properly evaluated. However, if the resistance can be estimated directly in-situ, the issue may be resolved.

In this paper, the results of four previous vibration tests are collected and reorganized. In the tests, schematically shown in Fig. 1, vibrations by the vibratory hammer of the sand compaction pile (SCP) method are applied to the ground and the accelerations induced in the ground and the generated excess pore water pressure are measured. Based on these results, the response of acceleration and excess pore water pressure at the sensor locations is correlated to the liquefaction resistance of the ground, from which a chart is developed to estimate the in-situ liquefaction potential of the ground improved by compaction.

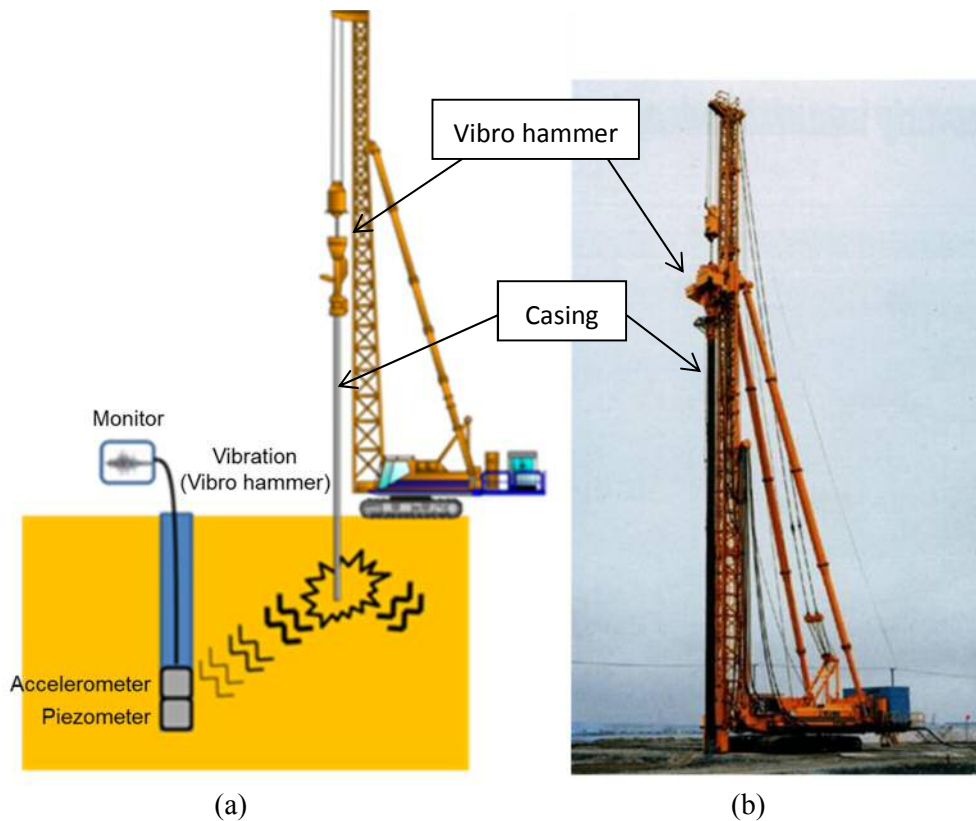


Fig. 1 – (a) Schematic diagram of vibration test; and (b) photo of vibro-hammer of SCP machine.



2. Re-analysis of previous vibration tests

2.1 Measurement conditions in previous vibration tests

In the past, attempts were made to evaluate the improvement effect in terms of water pressure control by comparing the excess pore water pressure (EPWP) developed in the original ground and the improved ground by directly measuring the in-situ pore water pressure within the ground. Table 1 summarizes the measurement conditions during the vibration tests at four sites: site A [2], site B [3], site C [4], and site D [5]. At sites A, B, and D, the casing of the SCP machine was used as vibration source (frequency: 9-10 Hz) and the generated acceleration and excess pore water pressure were measured. On the other hand, at site C, an H pile held by the vibro-hammer of the SCP machine was used as the vibration source. The table shows the location of the sensors (accelerometers and pore water pressure gauges), and the corresponding normalized N-value, N_1 , corrected N-value, N_a , and liquefaction resistance, R_L , computed from the SPT N-value and fines content, F_c , of the adjacent ground using Eq. (1) [6] and Eq. (2) [7]. The measurement points include the 4 locations in the original grounds and 6 locations in the improved grounds, resulting in a total of 10 measurement locations.

Table 1 – Measurement conditions in previous vibration tests

Site name	Set depth, z (m)	Ground	Specification (Infill material)	Fines content, F_c (%) ¹⁾	SPT N-value	Normalized N-value, N_1	Corrected N-value, N_a ²⁾	Liquefaction Resistance, R_L ²⁾	Remarks
Site A	4	Original ground (Fine sand)	–	19 (10)	7	10.7	10.7 (10.7)	0.221 (0.226)	*Measurement during installation (penetration/formation)
	7	Original ground (Fine sand)	–	19 (10)	5	6.1	6.1 (6.1)	0.167 (0.183)	
	7	Improved ground (Fine sand)	Unknown	19 (10)	15	18.3	18.3 (18.3)	0.291 (0.291)	
Site B	2	Original ground (Upper volcanic sand)	–	39.4	10	11.8	20.6 (25.9)	0.312 (0.451)	*Measurement during installation (penetration/formation) *Soil data from nearby data
	2	Improved ground (Upper volcanic sand)	700 □1.5m (sand)	38.2	15	17.7	29.3 (36.7)	0.709 (2.113)	
	8	Original ground (Lower volcanic sand)	–	35.2	7	6.2	10.7 (13.4)	0.221 (0.249)	
	8	Improved ground (Lower volcanic sand)	700 □1.5m (sand)	40.0	12	10.6	18.6 (23.6)	0.293 (0.371)	
Site C	4.5	Improved ground (Sandy soil)	700 □1.5m (sand)	10.0	25	34.1	34.1 (34.1)	3.132 (3.132)	* F_c measured from D_{50} and U_c [4]
	4.5	Improved ground (Sandy soil)	700 □1.6m (crushed stone)	10.0	22	30.0	30.0 (30.0)	0.795 (0.795)	
Site D	12.5	Improved ground (Sandy soil)	φ700 □1.6m (sand)	1033 (21.5)	31 (3170)	26.6	31.5 (34.7)	1.012 (1.734)	*Measurement at fixed position

¹⁾ F_c in () is average value

²⁾ N_a, R_L in () are from [7]



Design Specifications for Highway Bridges [6]:

$$R_L = \begin{cases} 0.088\sqrt{Na/1.7} & (Na < 14) \\ 0.088\sqrt{Na/1.7} + 1.6 \times 10^{-6}(Na - 14)^{4.5} & (Na \geq 14) \end{cases} \quad (1)$$

$$Na = C_1 N_1 + C_2$$

$$N_1 = 170N/(\sigma'_v + 70)$$

$$C_1 = \begin{cases} 1 & (0\% \leq F_c < 10\%) \\ (F_c + 40/50) & (10\% \leq F_c < 60\%) \\ F_c/20 - 1 & (F_c \geq 60\%) \end{cases}$$

$$C_2 = \begin{cases} 0 & (0\% \leq F_c < 10\%) \\ (F_c - 10)/18 & (F_c \geq 10\%) \end{cases}$$

Design Specifications for Highway Bridges [7]:

$$R_L = \begin{cases} 0.0882\sqrt{(0.85Na + 2.1)/1.7} & (Na < 14) \\ 0.0882\sqrt{Na/1.7} + 1.6 \times 10^{-6}(Na - 14)^{4.5} & (Na \geq 14) \end{cases} \quad (2)$$

$$Na = \begin{cases} C_{FC}(N_1 + 2.47) & (D_{50} < 2\text{mm}) \\ \{1 - 0.36\log_{10}(D_{50}/2)\}N_1 & (D_{50} \geq 2\text{mm}) \end{cases}$$

$$N_1 = 170N/(\sigma'_v + 70)$$

$$C_{FC} = \begin{cases} 1 & (0\% \leq F_c < 10\%) \\ (F_c + 20)/30 & (10\% \leq F_c < 40\%) \\ (F_c/16)/12 & (F_c \geq 40\%) \end{cases}$$

In the above equations, R_L is the liquefaction resistance, C_1 , C_2 , C_{FC} are the correction coefficients of the SPT N-value due to fines content, σ'_v is the effective overburden pressure (kN/m²) and D_{50} is the mean particle diameter (mm). Fig. 2 compares the liquefaction resistance for the 10 measurement points based on Eqs. (1) and (2). It is noted that the 2017 version of the code results in larger correction for fines content than the 1996 version; this is the aftermath of the results of investigations conducted following the 2011 Tohoku earthquake.

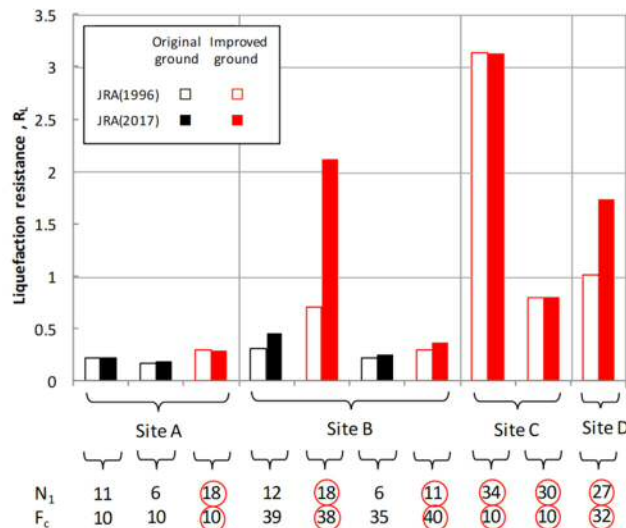


Fig. 2 – Comparison between the liquefaction resistance, R_L , at the 10 measurement points.

2.2 Outline and results of the test at site D

2.2.1 Outline of the experiment



To illustrate the vibration tests, site D is considered. Here, vibration was applied on the ground improved by the SCP method at a frequency of 9 Hz by oscillating a vibro-hammer using a casing, and the acceleration and the pore water pressure induced were measured over time through the accelerometer and pore water pressure gauge installed within the improved ground. Specifically, the accelerometer (with one vertical component and two horizontal components) and pore water pressure gauge shown in Fig. 3(a) were installed through the borehole at the position shown in Fig. 4, and shaking was applied by vibrating the vibro-hammer over a certain period of time near the sensors, at locations shown in Fig. 5. Fig. 3(b) shows the measurement condition at the time of the test. Fig. 4 also shows the cross-sectional view of the sensor installation location and the profile of the ground. The improvement pitch was \square 1.5 m (square grid pattern with improvement ratio, $a_s = 17.1\%$) and the soil profile consisted of an alternating layer of upper sand layer, lower sand layers (1) and (2), and clay layers. The sensor was installed at the lower sand layer (1) at GL-12.5 m.



Fig. 3 – Photos showing: (a) accelerometer and pore pressure gauge used in the test; and (b) condition during the test.

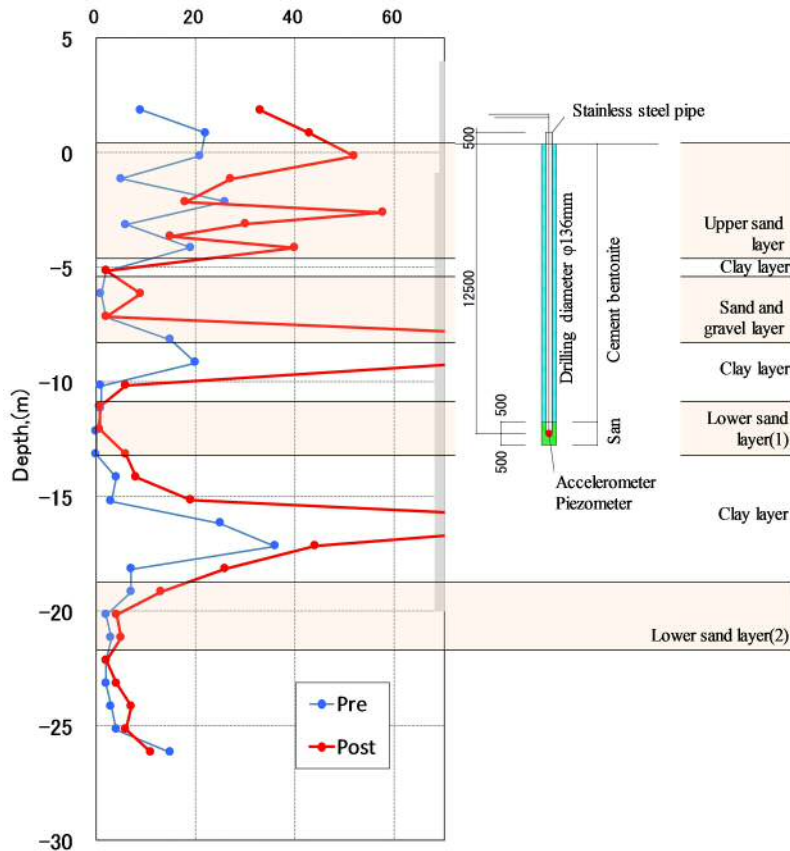


Fig. 4 – Cross-sectional soil profile and sensor location

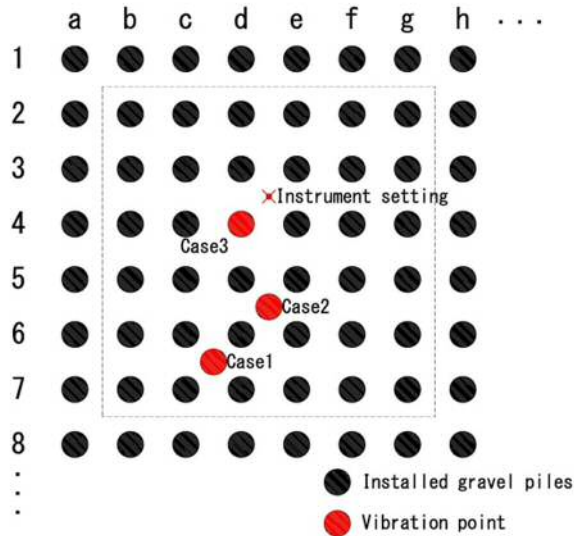


Fig. 5 – Layout of SCP piles and locations of sensors and vibration points for three cases at Site D

2.2.2 Measurement results

Fig. 6 shows the measurement results corresponding to the three locations where the vibration was induced (i.e. Cases 1-3). The time histories of the vertical acceleration (top row), horizontal acceleration (middle row) and excess pore water pressure (bottom row) are shown in the figure. Note that the vertical acceleration was



generally larger than the horizontal acceleration. In Cases 1 and 2, almost no excess pore water pressure was generated for the cases where the maximum vertical accelerations corresponded to 80 to 330 cm/sec^2 . In Case 3, where the largest vertical acceleration was measured at 1270 cm/sec^2 , the excess pore water pressure was only 24.1 kPa against an effective overburden pressure of 128 kPa (i.e., excess pore water pressure ratio, $r_u=0.19$).

Note that while actual earthquakes are generally multi-directional, it has been customary in practice to consider the horizontal peak ground acceleration, not the vertical acceleration, when evaluating liquefaction potential. This is because lateral shaking is a result of the propagation of S-wave into the medium (as compared to P-wave, which is generated by vertical acceleration). As a consequence, it is the horizontal peak ground acceleration which is used in the simplified empirical equation to calculate the shear stresses induced by the earthquake [6-7]. It should also be mentioned that numerical investigations performed by various researchers concluded that the resistance to liquefaction was not significantly affected by the vertical base acceleration [8, 9]. Hence, when investigating soil liquefaction occurrence in field tests, such as those discussed here, the horizontal peak acceleration, rather than the vertical peak acceleration, should be employed.

A comparison of both horizontal and vertical maximum accelerations recorded during vibration tests at Site D is shown in Fig. 7. It is clear that the maximum vertical accelerations are generally twice that of the maximum horizontal accelerations. Similar trends were observed at the other test sites; hence, the vertical accelerations dominate the observed response (due to the vertical vibration direction) and the maximum horizontal accelerations are about half of the maximum vertical accelerations.

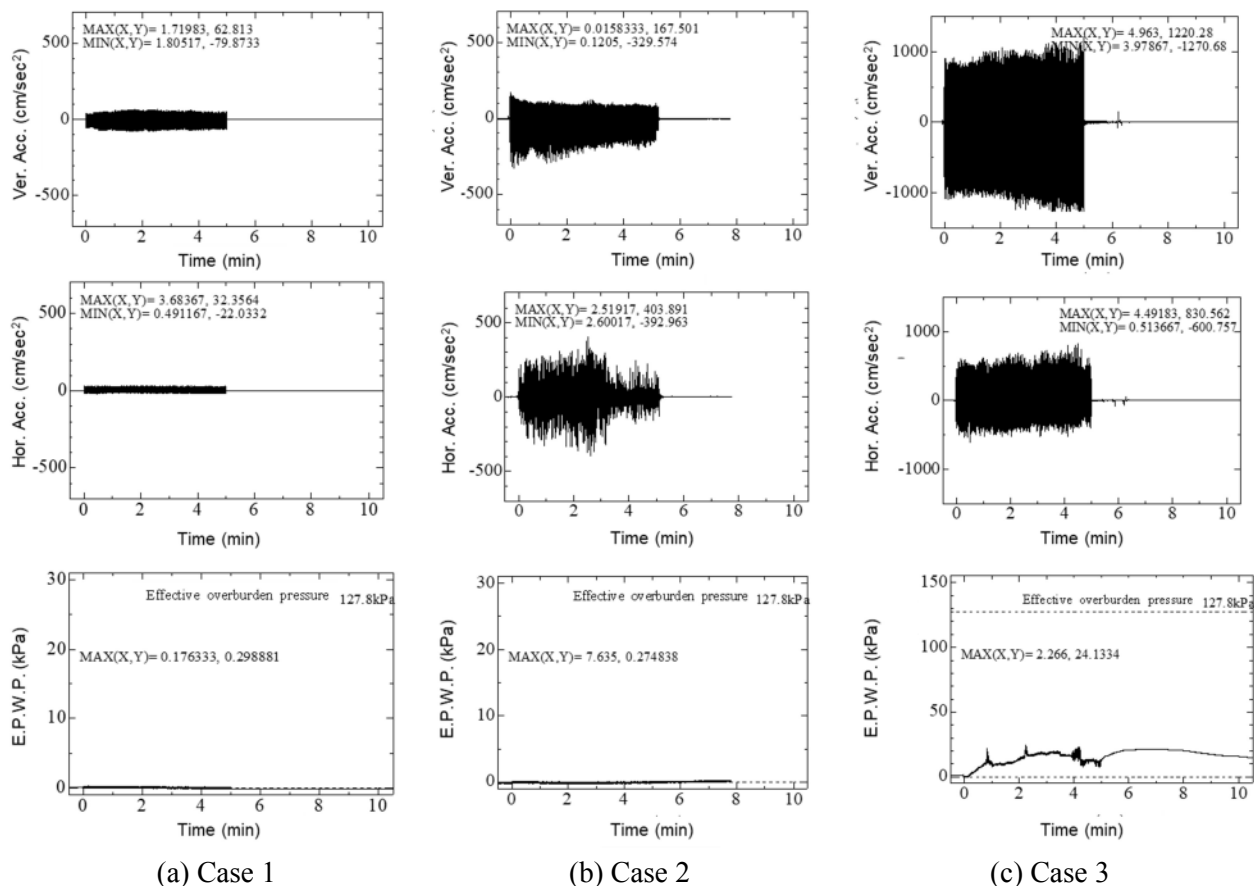


Fig. 6 – Time histories of vertical acceleration (top), horizontal acceleration (middle) and excess pore water pressure, EPWP (bottom) for each vibration point

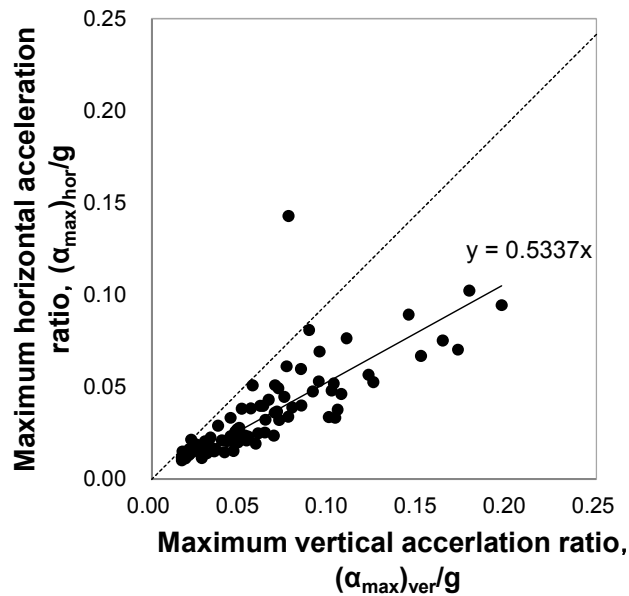


Fig. 7 – Comparison between maximum vertical and horizontal accelerations recorded at Site D.

3. Relation between acceleration due to vibration and excess pore water pressure

3.1 Confirmation of improvement effect

From the previous tests (sites A and B), the relations between the maximum horizontal acceleration ratio α_{max}/g and the maximum excess pore water pressure ratio, $r_{u,max}$ are plotted in Fig. 8. In terms of improvement effects, the three sets of data ($\circ \rightarrow \bullet$, $\Delta \rightarrow \blacktriangle$, $\square \rightarrow \blacksquare$) show that the range for the improved ground data plots to the right of the range for the original ground data. This trend indicates the effectiveness of ground improvement in suppressing the development of excess pore water pressure in the ground.

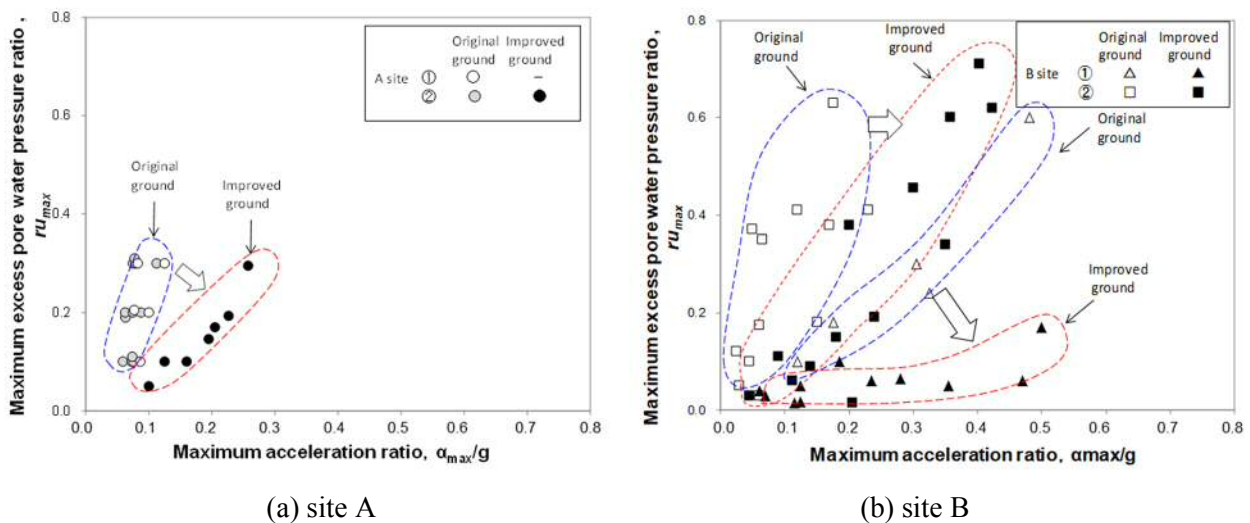


Fig. 8 – Results of vibration tests

3.2 Estimation of liquefaction resistance



The data of all the measurement points shown in Table 1 were divided into two groups: those with $F_c > 20\%$ and those with $F_c \leq 20\%$. For each group, the relations between the maximum shear stress ratio, L_{max} , obtained from the maximum horizontal acceleration ratio as indicated by Eq. (3), and the maximum excess pore water pressure ratio, $r_{u,max}$, are obtained and plotted in Fig. 9.

$$L_{max} = \frac{a_{max}}{g} \frac{\sigma_v}{\sigma_v'} \quad (3)$$

In the above equation, σ_v' and σ_v correspond to the effective and total overburden pressures, respectively, at the sensor installation depth. Note that while the maximum horizontal accelerations were monitored in sites A, B and D, no data was available for site C. Hence, the maximum horizontal accelerations in site C were estimated from the monitored maximum vertical accelerations and the relations shown in Fig. 7.

In the plots, the normalized SPT N values, N_1 , calculated using Eqs. (1) and (2), are also indicated beside each data point. Based on these values, trend lines corresponding to $N_1 = 5, 10$ for the original ground and $N_1 = 20, 30$ for the improved ground were drawn. Paying attention to the lines in both figures, it can be seen that lines with the same N_1 value tend to shift to the right as F_c increases. This is expected because higher fines content tend to suppress the generation of excess pore water pressure during shaking.

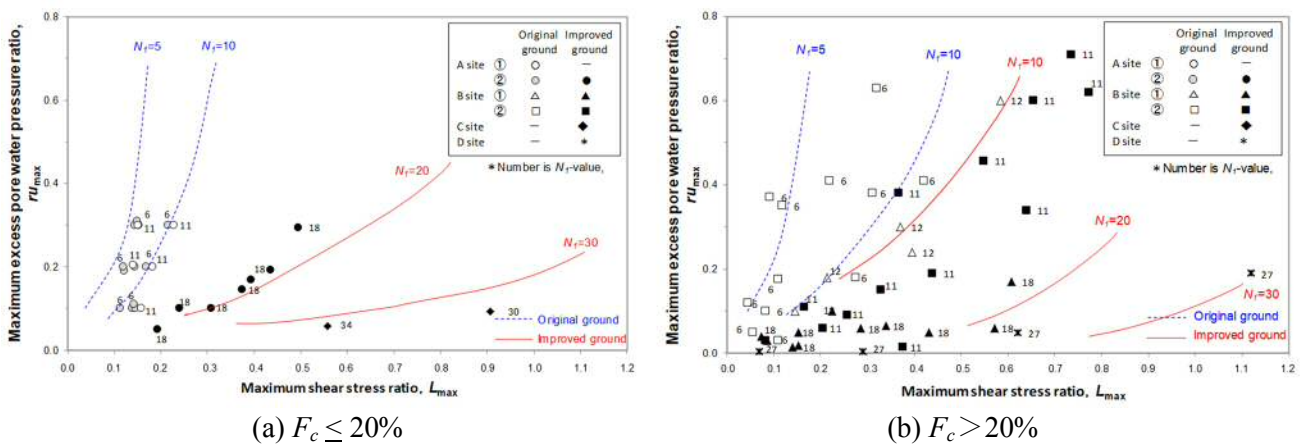


Fig. 9 – Relations between maximum shear stress ratio and excess pore water pressure ratio

To incorporate the effect of fines content, Fig. 10 shows the same plots, this time corresponding to the corrected SPT N value, N_a , calculated using Eqs. (1) and (2) from the codes [6, 7]. In the figure, the label for each data point is the N_a -value calculated using both codes. From these values, the trend lines for $N_a = 5, 10, 20$ for the original ground and $N_a = 20, 30$ for the improved ground, are drawn as in the previous figure. Considering the trend lines, it is seen that the water pressure suppression effect is different between the original ground and the improved ground even for the same $N_a = 20$ value, indicating that, for similar ground motion level, the improved ground has a higher pore water pressure reduction effect. This fact indicates that, for the same SPT N-value, the improved ground has larger liquefaction resistance when compared to the original ground. This is consistent with the observations from analysis examples based on N values and shear stress during actual earthquakes [10] as well as reproduction analysis examples of actual earthquakes [11].

Also indicated in the upper part of the figure are the ranges of liquefaction resistance, R_L , of the original ground estimated using both the 1996 and 2017 versions of the code [6, 7]. Note that when $ru_{max}=1.0$ for the original ground, the factor of safety against liquefaction, F_L , is equal to 1.0; hence, $L_{max}=R_L$. Thus, when the trend lines for the original ground are extended to $ru_{max}=1.0$, the lines should pass through these code-specified values. It can be observed that the extension of the trend lines for the original ground with $N_a=5$ and 10 generally fits the code specifications, while the line for $N_a=20$ plots more towards the right of the code-estimated values.



While more data is needed, it can be said that Fig. 10 provides a reasonable estimate of the liquefaction potential of both natural and SCP-improved grounds. That is, if L_{max} (expressed in terms of maximum horizontal acceleration ratio) and N_a of the ground at a particular depth are known, ru_{max} at that location can be estimated from the chart. Should a factor of safety against liquefaction, F_L , be required, this can be estimated using available F_L - ru relations [e.g. 12, 13]. Hence, the chart can be used to evaluate directly the in-situ liquefaction potential of both natural and SCP-improved grounds.

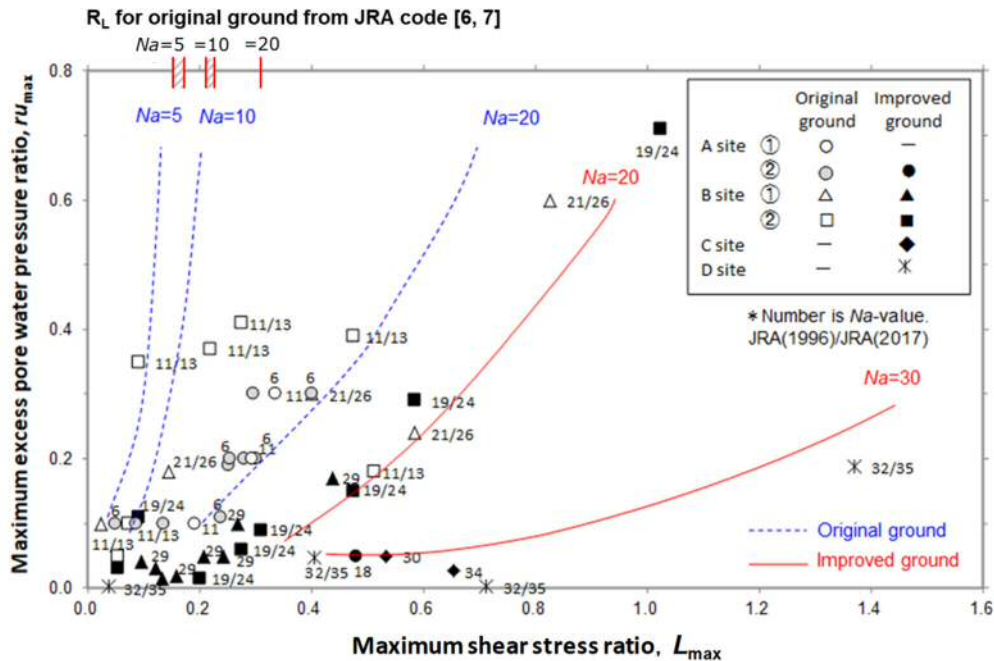


Fig. 10 – Chart for evaluating liquefaction potential

4. Conclusion

This paper collected and re-organized the results of previous vibration tests and proposed a chart (i.e. relation between the maximum horizontal shear stress ratio, L_{max} , and the maximum excess pore water pressure ratio, ru_{max}) for evaluating the in-situ liquefaction potential of both original and compacted ground. From the chart, it was found that the water pressure suppression effect was different between the original ground and the improved ground even for the same corrected N-value, N_a , with the improved ground having a higher water pressure reduction effect for the same ground motion level. This fact suggested that the improved ground had larger liquefaction resistance when compared to the original ground, consistent with the analysis examples based on N values and shear stress during actual earthquakes as well as reproduction analysis examples of real earthquakes.

References

- [1] Harada K, Ito T, Yamashita K (2018): Issues and responses on evaluation of improved ground by compaction. *Foundation Engineering & Equipment (Kiso-ko)*, **46** (11), 43-46 (in Japanese).
- [2] Ishihara K, Mitsui, S (1972): Field measurement of dynamic pore pressure during pile driving, *Proc., International Conference on Microzonation for Safer Construction*, 529-541.
- [3] Saito K, Degaki H, Senoo H (1981): Effects of liquefaction countermeasures using sand compaction piles. *Proc. 36th Annual Meeting of the Japan Society of Civil Engineers*, □-361, 720-721 (in Japanese).



- [4] Tottori T (1984): Liquefaction countermeasures for the Keiyo Line Viaduct, *Foundation Engineering & Equipment (Kiso-ko)*, **12** (7), 69-73 (in Japanese).
- [5] Yamashita K, Harada K, Ito T (2018): In-situ vibration tests on compacted ground, *Proc., 15th Japan Earthquake Engineering Symposium, 2029-2036* (in Japanese).
- [6] Japan Road Association (1996): Part V: Seismic Design. *Design Specifications for Highway Bridges* (in Japanese).
- [7] Japan Road Association (2017): Part V: Seismic Design. *Design Specifications for Highway Bridges* (in Japanese).
- [8] Ghaboussi J, Dikmen SU (1981): Liquefaction analysis for multidirectional shaking. *J. Geotech. Geoenviron. Eng.* **107**, 605–627.
- [9] Shiomi T, Yoshizawa M (1996). Effect of multi-directional loading and initial stress on liquefaction behaviour. *Proc., Eleventh World Conf. on Earthquake Engineering, Acapulco, Mexico*.
- [10] Asazuma R, Yoshitomi H, Harada K, Yamashita K (2018): Re-examination of evaluation of liquefaction resistance of improved ground by compacted sand pile method, *Proc., Architectural Institute of Japan Annual Meeting, Tohoku, 573-574* (in Japanese).
- [11] Harada K, Ishikawa K, Yasuda S, Nagai S (2016): An example of the evaluation of the effect of compaction improvement by the residual deformation evaluation method due to liquefaction, *Proc., Annual Meeting of Japan Society of Civil Engineers*, 437-438 (in Japanese).
- [12] Yasuda S (1985): Relationship between FL and excess pore water pressure ratio. *Proc. 21st Japanese Geotechnical Society Research Meeting*, 841-842 (in Japanese).
- [13] Ishikawa K, Yasuda S, Harada K (2013): Study on the excess pore water pressure ratio of various soil materials. *Proc. 33rd Earthquake Engineering Conference, ID2-430* (in Japanese).